

# Interaction of head model misspecification with EEG electrode density in the detection of regional brain signals



Mark E. Pflieger & Richard E. Greenblatt

*Source Signal Imaging, Inc., San Diego, USA*

## Introduction

The statistical power of detecting scalp EEG signals that originate *inside* a circumscribed brain region against a background of signals that originate *outside* the region depends on factors such as:

- Location and spatial extension of the brain region ([1], [2])
- Density and coverage of the scalp electrodes ([2], [3])
- Accuracy of the volume conductor model of the head (“head model”; [4], [5], [6])
- 3D registration errors; signal/noise characteristics; estimation algorithm; etc.

**Objective:** Within the framework of *regional activity estimation* (REGAE; [1]) we examine the tradeoff between regional signal discriminability and 3D resolution (spatial extension) for different brain locations as a function of both EEG electrode density and head model misspecification. Particular attention is paid to the *interaction* between the latter (i.e., between spatial sampling density and model inaccuracy).

## REGAE

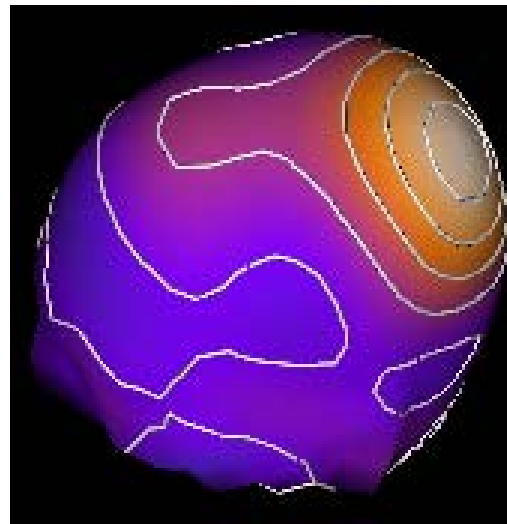
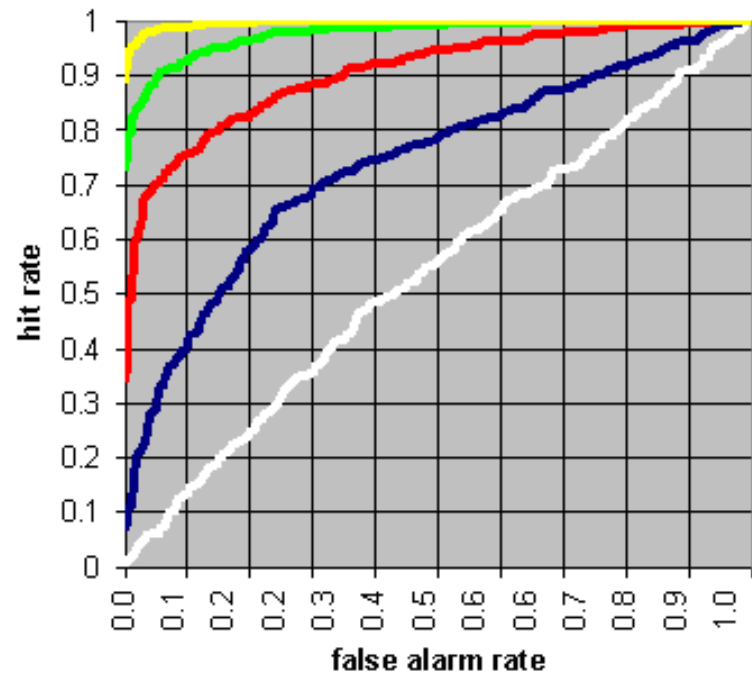
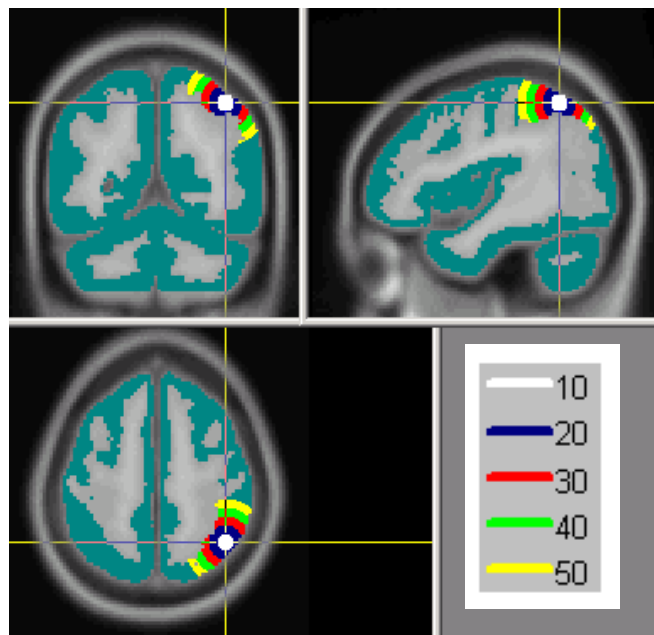
Regional activity estimation (REGAE) is a framework for detecting M/EEG signals that originate within specified brain regions of interest (ROIs).

For each ROI, REGAE seeks to optimize an inevitable tradeoff between *spatial resolution*, as measured by the spread of a region around a location in gray matter, and *discriminability* between intra-ROI and extra-ROI signals, as measured by the area under a suitably constructed receiver operator characteristic curve (AUROC). An ROI centered on a location has a minimum effective size, below which discriminability performance is no better than chance (AUROC = 0.5), and above which discriminability increases eventually to near perfect performance (AUROC = 1.0). Specific resolution/discriminability characteristics depend principally on the ROI location in the brain, the EEG electrode configuration, and the source space model of gray matter. Thus, in order to match (i.e., equalize) discriminability characteristics, spatial resolution must vary across brain regions.

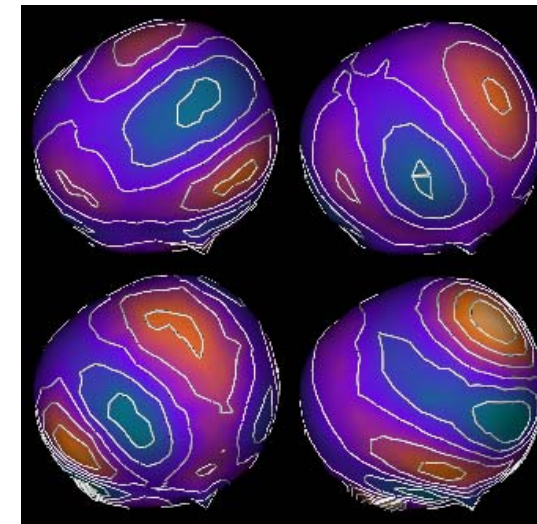
Figure 1 below illustrates these concepts. Shown are 3 ROIs with 5 spatial spreads (10 – 50 mm, FWHM), and their corresponding ROC curves. Discriminability (AUROC) increases with loss of spatial resolution (increase of spatial extension). Note that the parietal ROI has the best signal detection characteristics.

### Local vs. Global

A source estimator is *global* if it solves the global inverse problem, i.e., if the solution as a whole accounts for all of the scalp data (except noise). Prominent examples of global estimators are dipole modeling and distributed source modeling. A source estimator is *local* if it detects and/or estimates activity from a prespecified location (without attempting to solve the global inverse problem). REGAE is a local source estimator. Other local source estimators include the Backus-Gilbert method ([7], [3]), the Subtractive Optimally Localized Average technique (SOLA; [8]), and data adaptive beamformers ([9], [10], [11]).

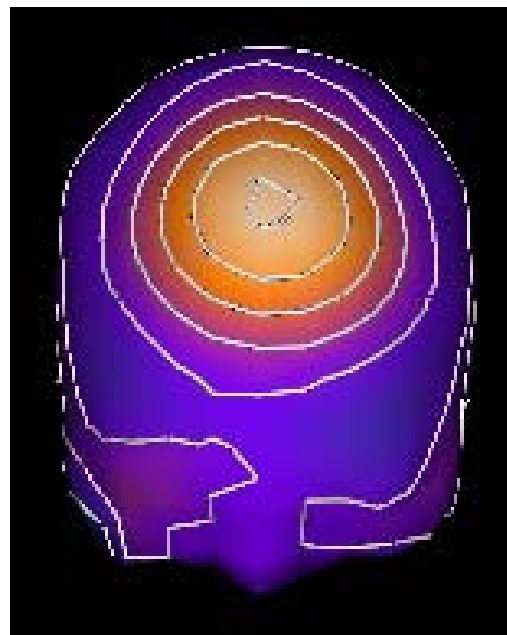
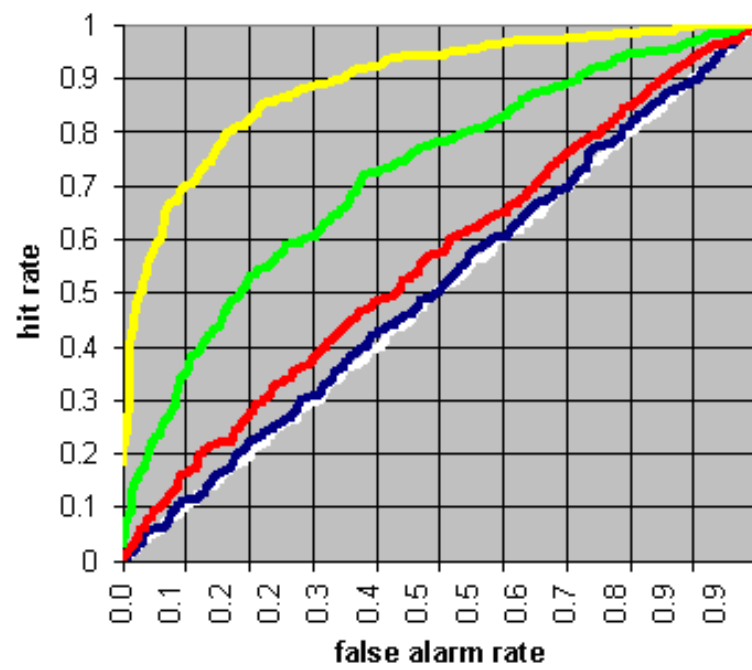
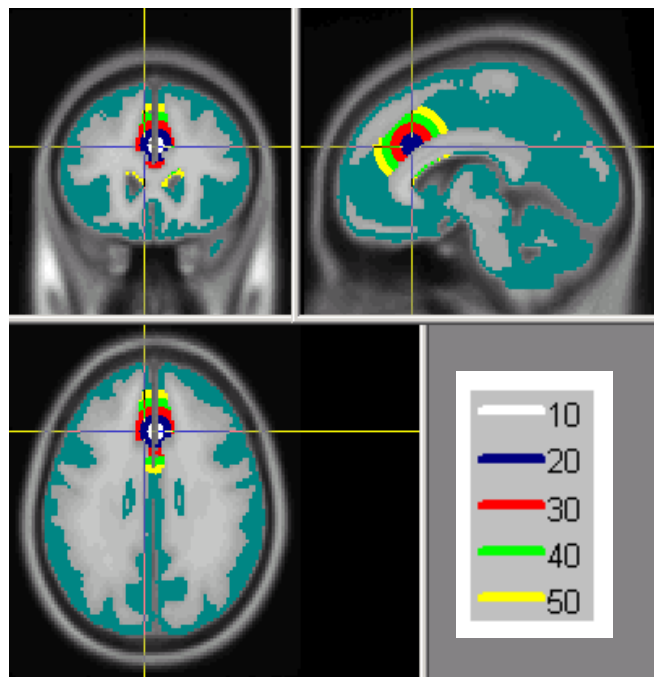


AUROC = 0.75, FWHM = 20 mm

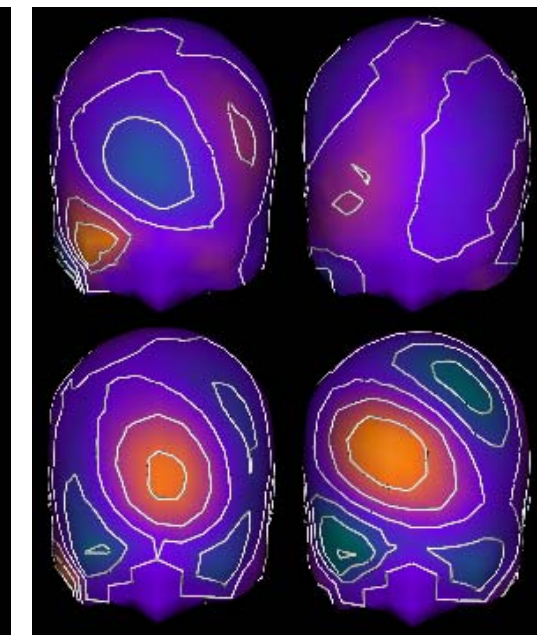


Relative weights: 6.45, 4.97, 3.72, 2.85

Figure 1a: **Left Parietal ROIs.** Left: Point of interest and 5 spatial spreads (10 – 50 mm FWHM; radiological convention). Middle: ROC curves for all spatial spreads. Right: Left rotated view of composite map and first 4 rows of ROI estimator, autoscaled.

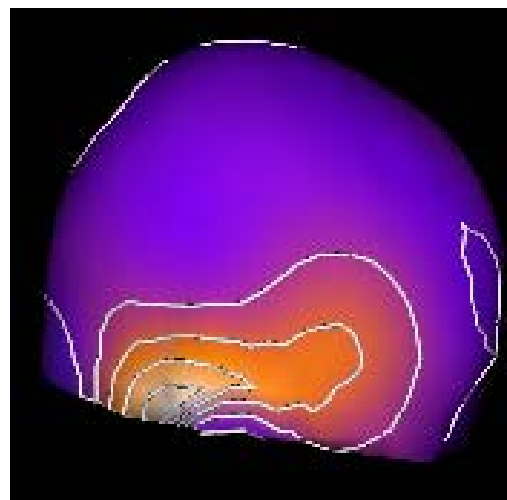
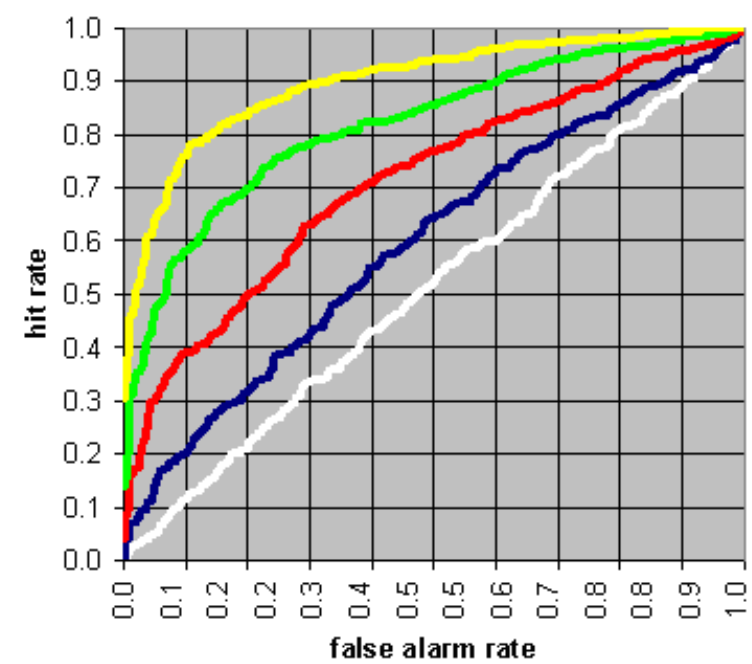
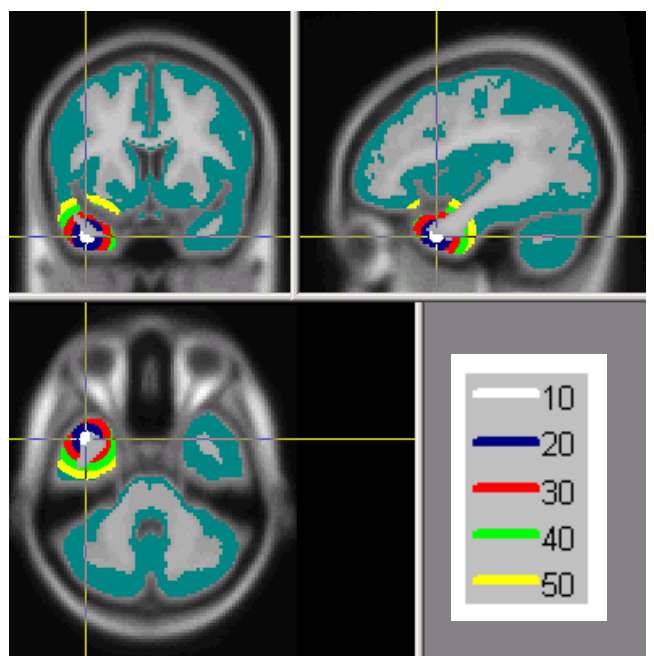


AUROC = 0.75, FWHM = 42 mm

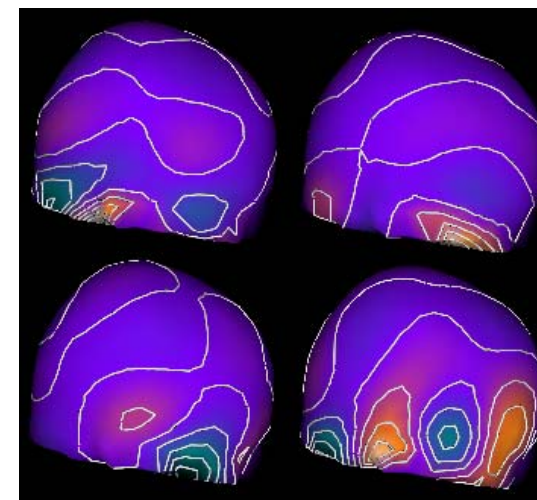


Relative weights: 14.7, 8.29, 6.6, 5.54

Figure 1b: **Bilateral ACC ROIs.** Left: Point of interest and 5 spatial spreads (10 – 50 mm FWHM; radiological convention). Middle: ROC curves for all spatial spreads. Right: Front tilted view of composite map and first 4 rows of ROI estimator, autoscaled.



AUROC = 0.75, FWHM = 33 mm



Relative weights: 7.89, 6.17, 3.28, 2.31

Figure 1c: **Right Temporal Pole ROIs.** Left: Point of interest and 5 spatial spreads (10 – 50 mm FWHM; radiological convention). Middle: ROC curves for all spatial spreads. Right: Right view of composite map and first 4 rows of ROI estimator, autoscaled.

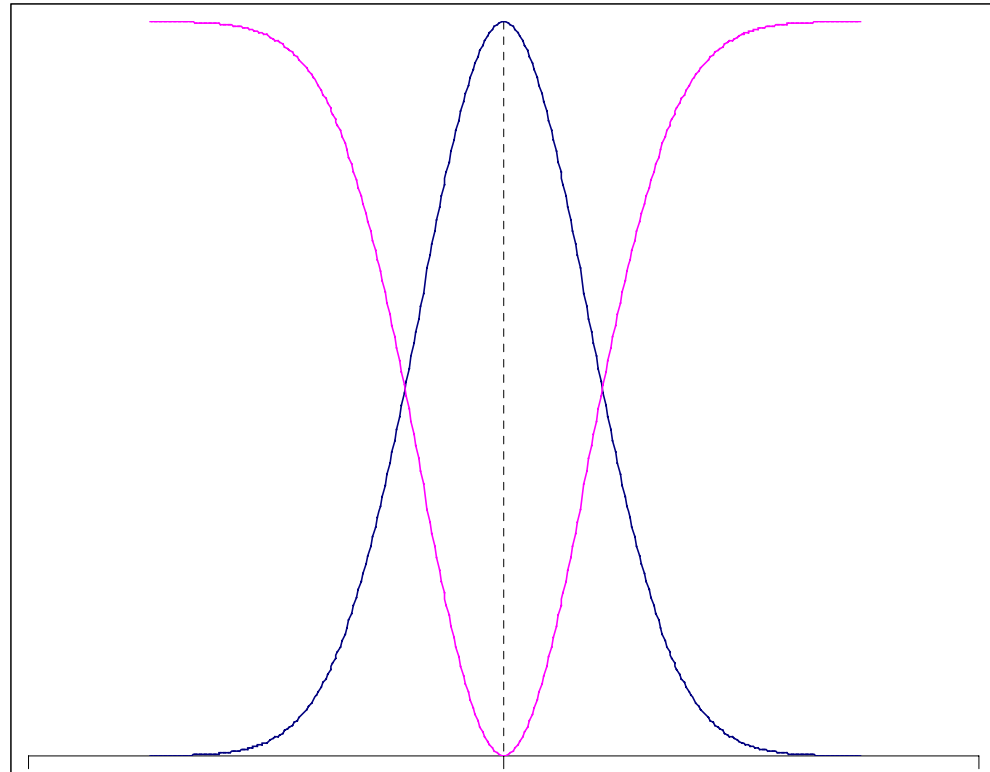


**Figure 2:** 1-dimensional illustration of a Gaussian “fuzzy” ROI (blue curve) and its complementary non-ROI (pink curve). The ROI is defined relative to a point of interest (POI) at the center. The full width at half maximum (FWHM) is the length between the points where the two curves intersect. The FWHM is approximately  $2.35 \sigma$  ( $\sigma$  = Gaussian standard deviation). In actual practice, the ROI is the intersection of the 3D Gaussian spread with the source space per figure 1.

**Computation of REGAE estimators:** A REGAE estimator for a region of interest (ROI) is a matrix  $\mathbf{E}$  of size  $d$  (estimation space dimension) by  $m$  (number of channels). The estimation space generally has more than one dimension because the region is spatially extended; this provides several degrees of freedom for current flow in gray matter. Given an EEG measurement  $\mathbf{v}(t)$  at time  $t$ , the ROI activity estimate at time  $t$  is  $\mathbf{E}\mathbf{v}(t)$ —a *vector* in  $d$ -dimensional estimation space. The *total* activity at time  $t$  is  $|\mathbf{E}\mathbf{v}(t)|$ , a non-negative scalar. To compute  $\mathbf{E}$ , first the source space is divided into ROI and non-ROI regions. A fuzzy region may be defined via a Gaussian distribution that surrounds a point of interest (POI) in 3 dimensions. Shown at left (figure 2) is a 1D ROI (blue) and its complementary non-ROI (pink). As illustrated above (figure 1), the ROI is the intersection of a Gaussian distribution with the source space (gray matter). Spatial spread may be measured via  $\sigma$ , the Gaussian standard deviation, or via the Gaussian full width at half maximum (FWHM). Assuming maximum entropy statistics on the source space (i.e., independent and identically distributed activity throughout), ROI and non-ROI covariance matrices are projected to the EEG measurement space via a volume conductor model of the head, and a ROI versus non-ROI *discrimination matrix* is formed from these two. The estimator matrix  $\mathbf{E}$  is obtained via singular value decomposition (SVD) of the discrimination matrix. A free parameter  $\gamma$ , useful for fine-tuning the ROC curve, is the power to which the singular values are raised. Estimation units are not physical units, but typically are normalized.

# Methods

## Source space

As illustrated in figure 1 (left column), we utilized a gray matter segmentation of the MNI-152 average head/brain for the source space. Three orthogonal current dipole elements were placed at 3152 locations within this segmented region.

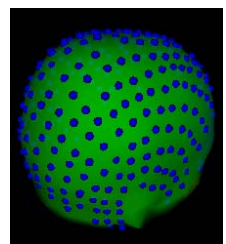
## Regions of interest

As shown in figure 1 (left column), ROIs were centered on three locations of interest in left parietal, bilateral anterior cingulate, right temporal pole cortices. The spatial extensions of regions used Gaussian spatial spreads of 5 – 50 mm FWHM (in 5 mm increments).

## Source signal statistics

Maximum entropy source signal statistics (unsmoothed Gaussian i.i.d.) were assumed.

## Measurement space



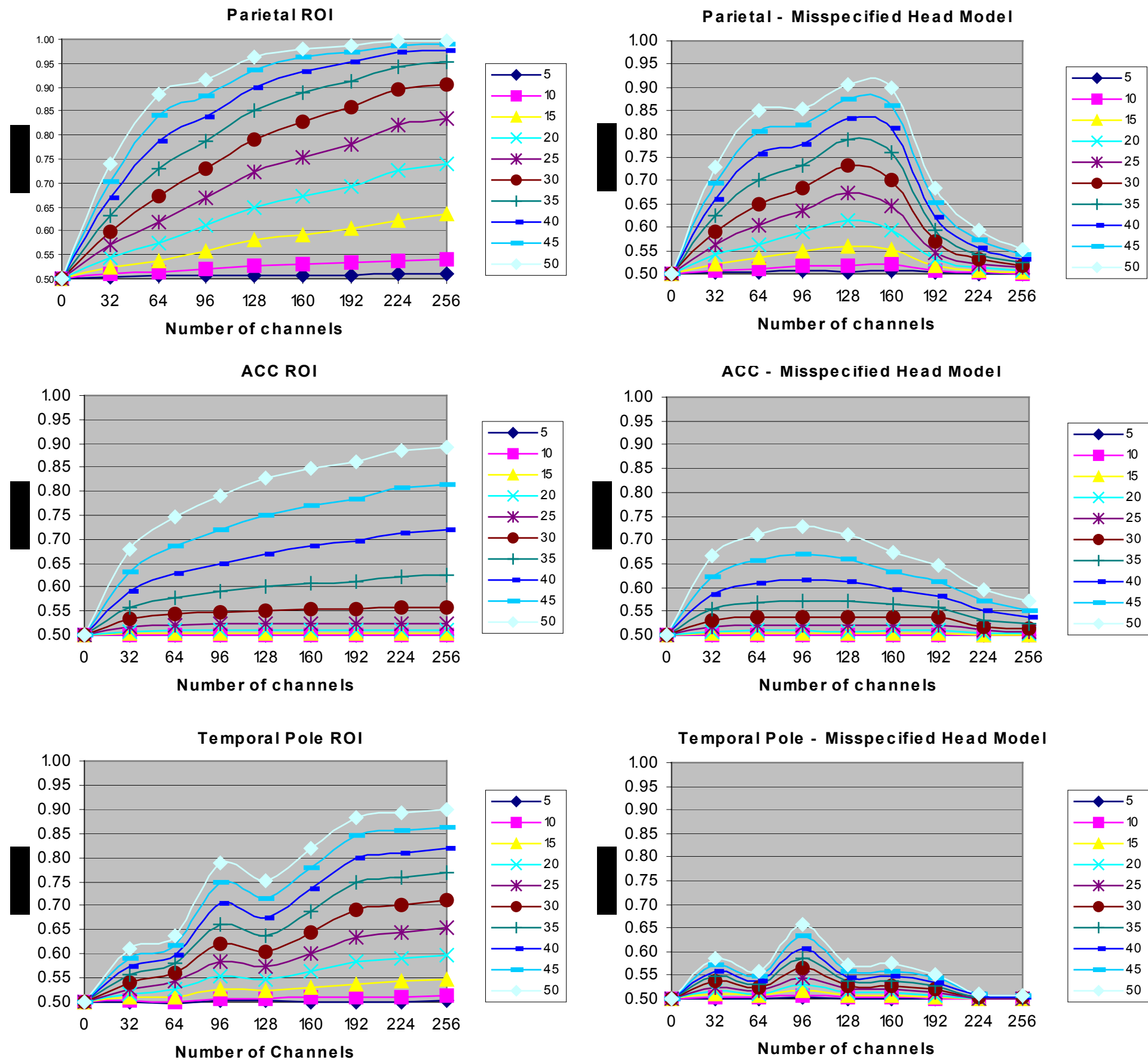
A digitization for a commercial 256-channel EEG system (Neuroscan ESI-256) was projected to the surface of the MNI-152 head. This was subsampled in increments of 32 channels using the following scheme: 32 = pick 1, skip 7; 64 = pick 1, skip 3; 96 = pick 3, skip 5; 128 = pick 1, skip 1; 160 = pick 5, skip 3; 192 = pick 3, skip 1; and 224 = pick 7, skip 1. A common average reference was utilized.

## Head models

3-shell sphere (best-fitting per electrode) and boundary element method (BEM) head models were utilized; geometries were derived from the MNI-152 average head.

## ROC curve generation

ROC curves were generated using the BEM head model to simulate data (a) with ROI plus non-ROI activity (to estimate the hit rate), and (b) with non-ROI activity only (to estimate the false alarm rate). The “ideal” case used the BEM to derive the REGAE estimator, whereas the “misspecified” case used the spherical model.



# Results

**Figure 3:** Families of curves for different spatial spreads (5 – 50 mm, FWHM) are plotted per ROI. In all cases, ROI discriminability performance (AUROC) increases monotonically with ROI spatial spread.

The *left column* shows the results of the *ideal* case, i.e., no head model misspecification. Except for one data point (128 channels, temporal pole ROI), AUROC increases monotonically with number of channels.

The *right column* shows the results of the *misspecified* head model case (BEM = actual, spherical = assumed model). Performance is generally degraded compared with the ideal case. However, *the most salient result is the downturn of ROI discriminability performance past a certain electrode density* (about 160 channels for the parietal ROI, and about 96 channels for the other two ROIs).

# Discussion

With an ideal (error-free) head model, ROI signal detection performance generally improves with increasing electrode density. Each ROI has its own profile. For the parietal ROI, near-perfect signal discrimination is achieved with a spread of 45 mm using 224 channels. For the anterior cingulate ROI, there is negligible improvement with electrode density for ROIs with spreads of 30 mm and less. The temporal pole ROI has an anomalous dip in performance at 128 channels, which can be explained in terms of the subsampling scheme: The “clumpy” 96-channel arrangement (pick 3, skip 5) by chance does a better job of representing the temporal pole than the more uniform 128-channel arrangement (pick 1, skip 1).

Although degradation of signal detection was expected for misspecified head models, we were initially surprised to observe the performance downturns at higher electrode densities. One hypothesis is that the REGAE estimator (which is optimized for the ideal case) becomes increasingly misled by higher spatial frequency content in the data when the head model is misspecified. An alternative hypothesis is that errors at all spatial frequencies contribute to the downturn, but are compounded when the discrimination matrix reaches a critical size.

In the continuation of this study, we are seeking to discriminate the alternative hypotheses with the aim of regularizing REGAE estimators in the presence of head model errors. In particular, we seek to optimize a regularizing linear derivation of the scalp channels. A related project seeks to estimate the actual errors that remain after realistic head modeling.

# References

- [1] Pflieger ME, Greenblatt RE (2001): A regional approach to M/EEG source estimation: Characterizing the tradeoff between spatial resolution and signal discriminability. *NeuroImage* 13(6): S219 (abstract).
- [2] MosherJC, Spencer ME, Leahy RM, Lewis PS (1993): Error bounds for EEG and MEG dipole source localization. *Electroencephalogr Clin Neurophysiol* 86: 303-21.
- [3] Pflieger ME, Nakada T (2000): The spatial resolving power of high-density EEG: an assessment of limits. In T Nakada (Ed.), *Integrated Human Brain Science: Theory, Method, Application (Music)*, Elsevier Science B.V., Amsterdam.
- [4] Jewett DL, Zhang Z (1995): Multiple-generator errors are unavoidable under model misspecification. *Electroencephalogr Clin Neurophysiol* 95(2): 135-42.
- [5] Awada KA, Greenblatt RE (1999): EEG source localization conductivity sensitivity using a 3D finite element model. *NeuroImage* 9:S138 (abstract).
- [6] Fuchs M, Kastner J, Wagner M, Hawes S, Ebersole JS (2002): A standardized boundary element method volume conductor model. *Clin Neurophysiol* 113(5): 702-12.
- [7] Press WH, Teukolsky SA, Vetterling WT, Flannery BP (1992): *Numerical Recipes in C (2<sup>nd</sup> Edition)*. New York: Cambridge University Press, pp. 815-8.
- [8] Pijpers FP, Thompson MJ (1994): The SOLA method for helioseismic inversion. *Astron Astrophys* 281:231-40.
- [9] Van Veen BD, van Drongelen W, Yuchtman M, Suzuki A (1997): Localization of brain electrical activity via linearly constrained minimum variance spatial filtering. *IEEE Biomed Eng* 44:867-80.
- [10] Robinson SE, Vrba J (1999): Functional neuroimaging by Synthetic Aperture Magnetometry (SAM). In T Yoshimoto et al. (Eds), *Recent Advances in Biomagnetism*. Sendai: Tohoku University Press, pp. 302-5.
- [11] Sekihara K, Nagarajan S, Poeppel D, Marantz A, Miyashita Y (2001): Reconstructing spatio-temporal activities of neural sources using an MEG vector beamformer technique. *IEEE Trans Biomed Eng* 48:760-1.

# Acknowledgment

We gratefully acknowledge the support of NIH grant 1R43MH64343-01.

## Citation

Pflieger ME, Greenblatt RE (2002): Interaction of head model misspecification with EEG electrode density in the detection of regional brain signals. Presented at the 8th International Conference on Functional Mapping of the Human Brain, June 2-6, 2002, Sendai, Japan. Available on CD-ROM in *NeuroImage*, Vol. 16, No. 2.